PHYSICAL REVIEW B **81**, 060407(R) (2010)

Self-organized structures of orbital-ordered domains in $Nd_{1-x}Sr_{1+x}MnO_4$

T. Nagai,[1] T. Kimura,[2] T. Asaka,[3] K. Kimoto,[1,4] M. Takeguchi,[1,4] and Y. Matsui[4]

[1]*Transmission Electron Microscopy Cluster, National Institute for Materials Science (NIMS), Tsukuba 305-0047, Japan*

[2]*Division of Materials Physics, Graduate School of Engineering Science, Osaka University, Toyonaka, Osaka 560-8531, Japan*

[3]*Nanostructures Research Laboratory, Japan Fine Ceramics Center (JFCC), Nagoya 456-8587, Japan*

[4]*Advanced Electron Microscopy Group, National Institute for Materials Science (NIMS), Tsukuba 305-0044, Japan*

(Received 26 November 2009; published 16 February 2010)

Self-organizing domain structures of charge-orbital-ordered (COO) and ferro-orbital-ordered (FOO) phases were observed for tetragonal layered manganites $Nd_{1-x}Sr_{1+x}MnO_4$ ($x=0.8$ and 0.82) by low-temperature transmission electron microscopy. We revealed a marked temperature variation of coexisting COO domains with equivalent structural distortions and orbital ordering patterns at $x=0.8$. The observed competition of coexisting FOO domains at $x=0.82$ also clearly reflects the self-organizing nature of e_g electrons. Furthermore, a checkered structure, in which COO domains were reproduced at the intersections of FOO domains, was found in the transition from the COO phase to the FOO phase at $x=0.8$. The observations suggest that strain energy affects the self-organizing behavior in the orbital ordering.

DOI: 10.1103/PhysRevB.81.060407 PACS number(s): 75.60.Ch, 71.27.+a, 61.50.Ks, 68.37.Lp

There has been growing recognition that the self-organizing behavior of electrons and the resulting nanometer- and micrometer-scale phase separations play a key role in various phenomena, such as superconductivity and colossal magnetoresistance (CMR), in strongly correlated electron systems.[1,2] In particular, phase separation and competition between paramagnetic insulating, ferromagnetic metallic, and charge-orbital-ordered (COO) insulating phases in manganites have been intensively studied owing to the CMR effect.[3–6] Strain fields and chemical disorder have been suggested as the origins of the coexistence of these phases,[7–9] and a theoretical study incorporating primarily the structural aspects has predicted that micrometer-scale multiphase coexistence is self-organized and is caused by the presence of an intrinsic elastic energy landscape.[10] In this Rapid Communication, we present a real-space observation of self-organizing orbital domain structures in tetragonal single-layered manganites $Nd_{1-x}Sr_{1+x}MnO_4$ ($x=0.8$ and 0.82) by low-temperature transmission electron microscopy (TEM). The marked temperature variations of coexisting orbital-ordered domains with equivalent structural distortions and orbital ordering patterns clearly reflect the self-organizing nature of e_g electrons. Moreover, we found a checkered structure, in which COO domains were reproduced at the intersections of ferro-orbital-ordered (FOO) domains, in the transition from the COO phase to the FOO phase. The observations suggest that strain energy affects the self-organizing behavior in the orbital ordering.

$Nd_{1-x}Sr_{1+x}MnO_4$ single crystals ($x=0.8$ and 0.82) were grown by the floating zone method with a halogen-lamp image furnace in flowing air. TEM specimens were prepared by ion milling. Selected-area electron-diffraction (SAED) patterns and bright-field (BF) and dark-field (DF) images were obtained using a Lorentz transmission electron microscope (Hitachi HF-3000L) operated at 300 kV and equipped with a liquid-nitrogen-type low-temperature sample holder. We performed x-ray diffraction and SAED measurements, which show that the basic structure is of the K_2NiF_4 type with $I4/mmm$ tetragonal symmetry. The physical properties and electric phase diagram of the $Nd_{1-x}Sr_{1+x}MnO_4$ system ($0.67 \leq x \leq 1.0$) are described in detail in Ref. 11.

The tetragonal symmetry of basic structure gives rise to multiple coexisting orbital-ordered domains, which have equivalent Jahn-Teller distortions and orbital ordering patterns. Our structural investigation revealed that four shear-type Jahn-Teller modes occur in the $Nd_{1-x}Sr_{1+x}MnO_4$ system, as schematically illustrated in Fig. 1(a).[12] The relative shifts of oxygen atoms from the tetragonal positions are along $[1\bar{1}0]$ in the $x1$ and $y1$ modes, whereas those are along $[1\bar{1}0]$ in the $x2$ and $y2$ modes. The $x1$ and $x2$ modes increase the Mn-O distance along the x direction and stabilize the $3x^2-r^2$ orbital. On the other hand, the $y1$ and $y2$ modes increase it along the y direction and stabilize the $3y^2-r^2$ orbital. Two types of COO domains with equivalent Jahn-Teller distortions and $3x^2-r^2/3y^2-r^2$ antiferro-orbital ordering patterns are realized in this system, as illustrated in Fig. 1(b). The high-resolution TEM study revealed that the COO states are accompanied by sinusoidal and transverse structural modulations with the modulation vectors $[\delta, \pm\delta, 0]$ $[\delta \approx (1-x)/2]$.[12] Wigner-crystal-type ordering patterns are proposed on the basis of the results of TEM observation and resonant x-ray scattering.[13] In the $x=0.8$ sample, the period of structural modulation (d_{COO}) is 2.5 nm with $\delta=0.108$ at 108 K. MnO_6 octahedra are distorted in the $x1$ and $y1$ modes in the α domain with the modulation vector (q_α) parallel to $[1\bar{1}0]$ and in the $x2$ and $y2$ modes in the β domain with the vector (q_β) parallel to [110]. Similarly, four FOO phases with equivalent structural distortions are realized, as illustrated in Figs. 1(c) and 1(d). Previous neutron and x-ray diffraction studies on $Nd_{1-x}Sr_{1+x}MnO_4$ with $0.75 < x < 0.9$ revealed that the lattice deformation which increases the Mn-O distance along a unique direction, x or y, originates from the FOO states.[11,14] SAED measurements showed that the symmetry of the distorted structures is monoclinic. The octahedra are distorted in the $x1$, $y1$, $x2$, and $y2$ modes in the $3x^2-r^2$ FOO α, $3y^2-r^2$ FOO α, $3x^2-r^2$ FOO β, and $3y^2-r^2$ FOO β domains, respectively.

Figure 2(a) shows the temperature dependence of satellite reflections in the $x=0.8$ sample. The electron beam is incident along the [001] zone axis in the selected area of 320 nm diameter. Upon cooling from room temperature (RT), very weak and broad satellite reflections with the modulation vec-

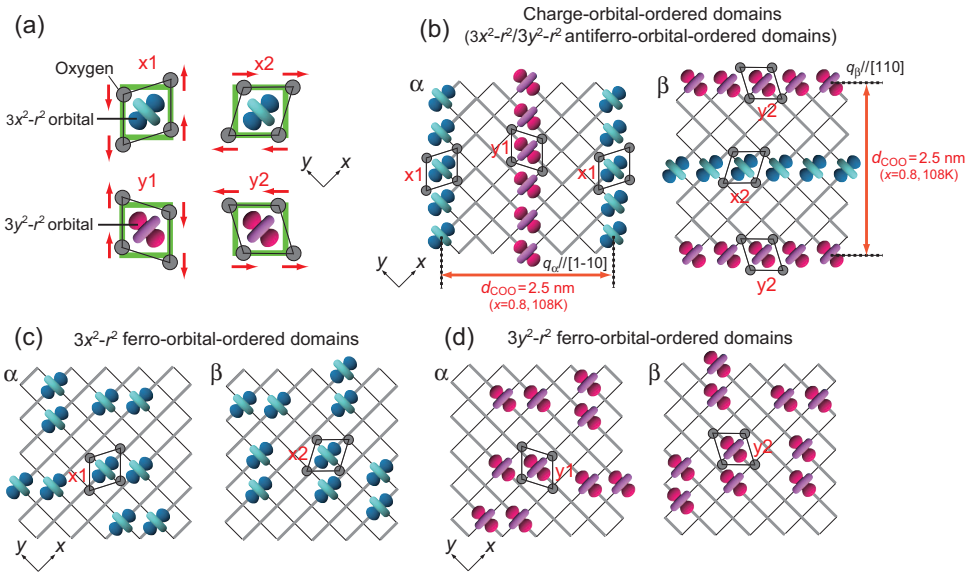

FIG. 1. (Color) Schematic illustration of COO and FOO states accompanied by four shear-type modes of MnO_6 Jahn-Teller distortion in $Nd_{1-x}Sr_{1+x}MnO_4$. (a) $x1$, $x2$, $y1$, and $y2$ modes of MnO_6 distortion. (b) COO states with $3x^2-r^2/3y^2-r^2$ antiferro-orbital order in COO α domain ($q_\alpha \| [1\bar{1}0]$) and COO β domain ($q_\beta \| [110]$). (c) $3x^2-r^2$ FOO states in α domain ($x1$ mode) and β domain ($x2$ mode). (d) $3y^2-r^2$ FOO states in α domain ($y1$ mode) and β domain ($y2$ mode). The charge is disordered in all the FOO domains.

tors parallel to $[1\bar{1}0]$ and [110] appear at around 260 K. The two sets of superlattice reflections with q_α and q_β are induced by the COO α and COO β domains, respectively. The intensity increases and the full width at half maximum (FWHM) decreases progressively with decreasing temperature. However, the superlattice reflections with q_α disappear at around 190 K. We can observe a marked change in real space in the DF images using the $(2a^*+q_\alpha)$ reflection, as shown in Fig. 2(b). The circle shows the selected area in the diffraction measurements. Although weak granular contrasts of the α domains cover the specimen area at 220 K, the contrasts are completely turned away from the area at 160 K. The temperature dependence of the β domains is observed in the DF images using the $(2a^*+q_\beta)$ reflection [Fig. 2(c)]. This self-organizing behavior should be closely related to the amplitude of Jahn-Teller distortion and the coherent length of charge-orbital order. The intensity of the superlattice reflections reflects the amplitude of distortion, which has been demonstrated by our simulation study.[12,15] The FWHM of superlattice reflections and the contrasts of images show the coherent length. At the higher temperature, the two parameters and elastic energy are very small, and hence, the COO domains can occur almost everywhere in the specimen. At the lower temperature, by contrast, the parameters and energy are large, and therefore, the stability of the COO domains probably depends on strain fields in the specimen. Accordingly, domains of one COO state survive and grow, and those of the other COO state deteriorate in wide areas of the specimen.

A similar self-organizing behavior can be observed in the FOO phases. Figure 3(a) shows the temperature dependence of the 2–20 fundamental reflection in the [001] SAED pattern of the $x=0.82$ sample. Upon cooling from RT, the reflection becomes streaked along [110] and the intensity distribution along the direction changes into a trapezoid pattern at around 190 K. With a further decrease in temperature, the distribution changes into a double-peak pattern and two monoclinic reflections are separated. The upper and lower reflections originate from the $3y^2-r^2$ and $3x^2-r^2$ FOO β domains, respectively. Figure 3(b) shows the temperature variation of the BF images in exciting the upper part of the highly streaked reflection. The bright and dark areas correspond to the $3x^2-r^2$ FOO β and $3y^2-r^2$ FOO β domains, respectively. Nanobeam electron-diffraction measurements indicate that the streaked reflection consists of a number of reflections induced by narrow domains with different degrees

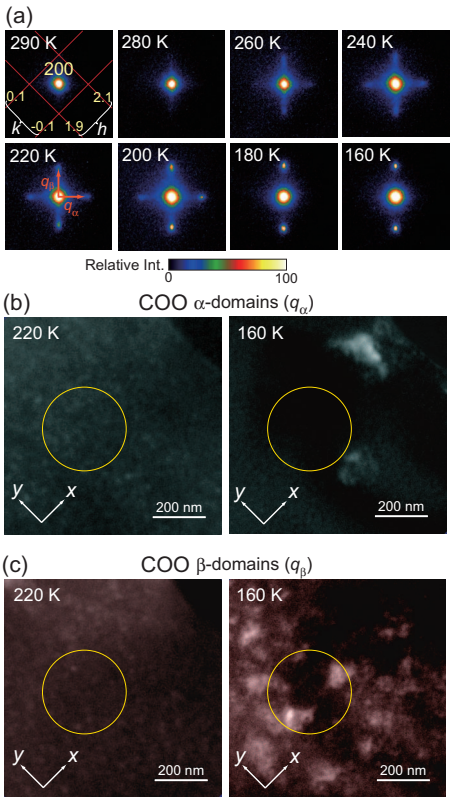

FIG. 2. (Color) Self-organizing COO domain structure at $x=0.8$. (a) Temperature dependence of satellite reflections around 200 fundamental reflection in [001] zone axis selected-area electron-diffraction (SAED) pattern. (b) DF images observed using $(2a^*+q_\alpha)$ reflection induced by COO α domains. (c) DF images observed using $(2a^*+q_\beta)$ reflection induced by COO β domains. Circles show the selected area in the diffraction measurements.

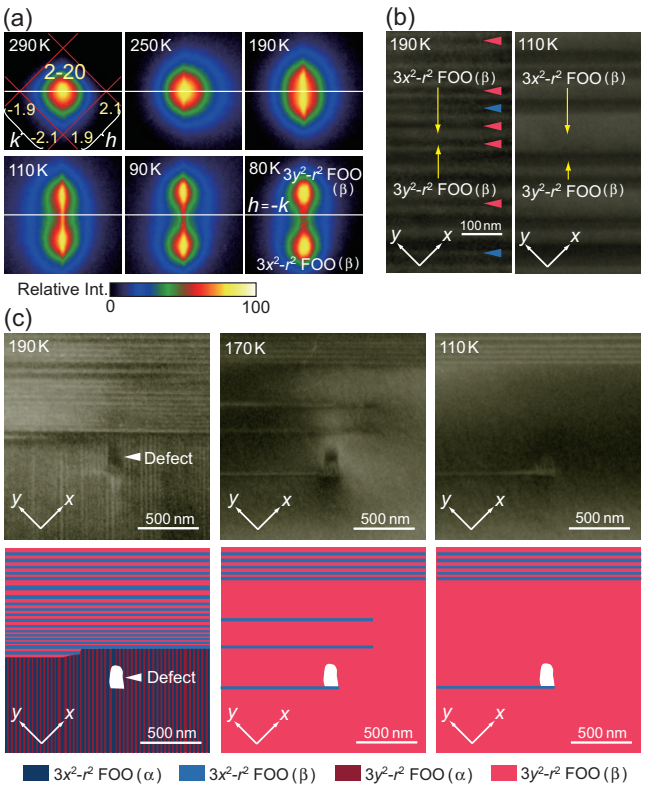

FIG. 3. (Color) Self-organizing FOO domain structures at $x=0.82$. (a) Temperature dependence of 2–20 fundamental reflection in [001] zone axis SAED pattern. (b) BF images observed in exciting upper part of highly streaked reflection. The bright and dark bands correspond to the $3x^2-r^2$ and $3y^2-r^2$ FOO β domains, respectively. The $3x^2-r^2$ FOO β domains indicated by blue arrows and the $3y^2-r^2$ FOO β domains indicated by red arrows deteriorate with decreasing temperature. (c) Temperature dependence of BF images obtained for an area where four types of FOO domains coexist at 190 K. The dark area indicated by an arrow shows a crystal defect. A schematic illustration of the domain structures is shown in the lower panel.

of distortion. When the position of reflection caused by one domain is described as $(2+A,-2+A,0)$, the distortion increases with increasing $|A|$. With decreasing temperature, the bands indicated by arrows deteriorate and the other bands grow instead; consequently, the width of the bands increases. The position of reflection indicates the amplitude of Jahn-Teller distortion, and the width of the bands shows the coherent length of ferro-orbital order. The stability of the FOO domains becomes dependent on strain fields because of the large elastic energy with decreasing temperature.

We found a marked change in domain structure in an area where the four types of FOO domains coexist at 190 K. The upper left, middle, and right images in Fig. 3(c) are BF images obtained at 190, 170, and 110 K in the $x=0.82$ sample. Upon cooling from 190 K, the $3x^2-r^2$ and $3y^2-r^2$ FOO α domains were suddenly replaced by a wide $3y^2-r^2$ FOO β domain. Simultaneously, some of the $3x^2-r^2$ FOO β domains were replaced by the wide $3y^2-r^2$ FOO β domain. One narrow $3x^2-r^2$ FOO β domain formed in contact with a crystal defect and remained at 110 K, although the nearby $3x^2-r^2$ FOO β domains disappeared above 110 K. These images show that the local strain fields around the defect affect the orbital state through the Jahn-Teller effect and pinned the $3x^2-r^2$ FOO β domain.

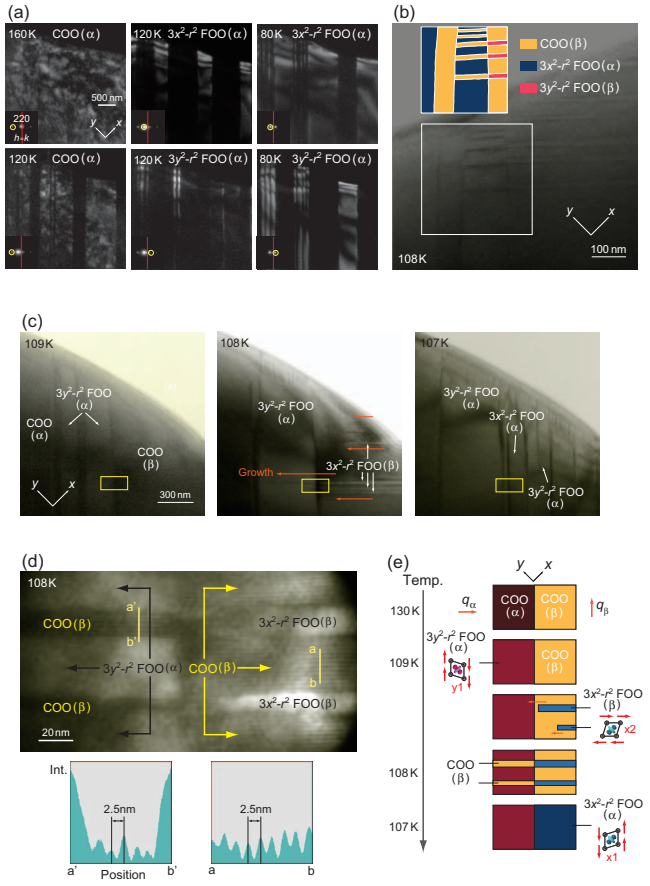

FIG. 4. (Color) Self-organizing COO and FOO domain structures in the transition from the COO phase to the FOO phase at $x=0.8$. (a) Temperature dependence of DF images obtained for an area covered by COO α domains at 160 K. The insets show the reflections used. (b) The BF image observed at 108 K shows a checkered domain structure. The inset illustrates the domain structure in the area marked by a white line. (c) Temperature dependence of BF images obtained for area where COO α and COO β domains coexist at 109 K. (d) BF image obtained at 108 K for area marked by a yellow line in (c). The intensities of the images on the a-b and a'-b' lines are displayed in the lower panel. Two COO β domains are reproduced at the intersections of $3x^2-r^2$ FOO β and $3y^2-r^2$ FOO α domains. (e) Schematic illustration of temperature dependence of domain structure in area marked in (c).

SAED measurements showed that COO and FOO phases coexist at $\sim$140–100 K, and the COO phase disappears below $\sim$100 K in the $x=0.8$ sample. Figure 4(a) shows the DF images showing the temperature dependence of the domains in an area covered by the COO α domains at 160 K. With decreasing temperature, stripelike $3x^2-r^2$ and $3y^2-r^2$ FOO α domains emerge and grow, while the COO α domains deteriorate. The relative shifts of oxygen atoms from the tetragonal positions are parallel to [110], which is perpendicular to the modulation vector of the COO domains, in all the coexisting domains. The relationship between the relative shifts and the modulation vector is also confirmed in the areas covered by the COO β domains. The same lamel-

lar phase separation has been observed for $La_{1-x}Ca_xMnO_3$ by Tao *et al.*[16] and Loudon and Midgley.[17] Around the boundary between the COO α and COO β domains, we found a checkered domain structure, as shown in Fig. 4(b). This structure is metastable and suddenly collapses with decreasing temperature. Figure 4(c) shows the temperature dependence of the structures of the COO and FOO domains in another area. The BF image obtained at 109 K shows an area around the boundary between the COO α and COO β domains, including the $3y^2-r^2$ FOO α domains that have been transformed from the COO α domain. Upon cooling below 109 K, narrow $3x^2-r^2$ FOO β domains emerge around the edge of the specimen and rapidly grow along $[\bar{1}10]$. Simultaneously, the $3y^2-r^2$ FOO α domain also grows in the middle of the area. As soon as the $3x^2-r^2$ FOO β domain reaches the boundary between the $3y^2-r^2$ FOO α domain and the COO β domain, a COO β domain with the same width emerges instead from the $3y^2-r^2$ FOO α domain and grows along $[\bar{1}10]$. Figure 4(d) shows a BF image obtained at 108 K for the area marked by a yellow line in Fig. 4(c), clearly showing the checkered domain structure. The intensities of the images on the *a*-*b* and *a*′-*b*′ lines show the superlattice fringe caused by COO structural modulation with a period of 2.5 nm, as shown in the lower panel. On further cooling, all the COO β domains are suddenly replaced by the $3x^2-r^2$ and $3y^2-r^2$ FOO α domains, and the checkered structure concomitantly vanishes. The process of appearance and disappearance of the checkered domain structure in the marked area is illustrated in Fig. 4(e).

We confirmed that a COO domain always forms at the intersection of a $3x^2-r^2$ FOO domain and a $3y^2-r^2$ FOO domain. There are two domain combinations that reproduce a COO domain: (1) $3x^2-r^2$ FOO β and $3y^2-r^2$ FOO α domains, and (2) $3x^2-r^2$ FOO α and $3y^2-r^2$ FOO β domains. Any COO domain does not occur at the intersection of two $3x^2-r^2$ FOO domains or two $3y^2-r^2$ FOO domains. These observations imply that the two kinds of strain with crossing directions relax the monoclinic distortion and reproduce a COO domain in the overlapping region. A similar domain structure has been observed in martensite systems. It has been reported that the intersections of two hcp ε-martensite variants retain the fcc parent phase symmetry in Fe-Mn-Si shape memory alloy.[18,19] The phase transition from the fcc matrix to hcp martensite is accomplished by shear deformation, which is the same as in our case. The checkered structure indicates that the reaction kinetics is dominated by strain energy; the lattice deformation accompanies a shape change in the transforming area, which should be accommodated elastically within the crystal.

The presented self-organizing behavior in COO and FOO phases and the transition process are indicative of the essential feature that strain energy affects the behavior of e_g electrons. The effect is enhanced at lower temperatures because the amplitude of distortion and the coherent length increase with decreasing temperature. The pinning of an FOO domain by a crystal defect demonstrates the importance of strain fields. The self-organizing nature of e_g electrons realizes the checkered domain structure, where the total elastic energy is reduced by the reproduction of COO domains at the intersections of FOO domains.

In conclusion, we have presented the real-space imaging of self-organizing structures of charge-orbital-ordered and ferro-orbital-ordered domains in the tetragonal manganites $Nd_{1-x}Sr_{1+x}MnO_4$ ($x=0.8$ and 0.82) by low-temperature TEM. The obtained results suggest that the self-organizing nature of electrons to minimize the elastic energy is important for phase separation and competition in orbital-ordered manganites.

We thank X. Z. Yu and W. Zhang for experimental support. This work was partly supported by a Nanotechnology Network Project from MEXT, Japan.

[1] S. H. Pan, J. P. O'Neal, R. L. Badzey, C. Chamon, H. Ding, J. R. Engelbrecht, Z. Wang, H. Eisaki, S. Uchida, A. K. Guptak, K.-W. Ng, E. W. Hudson, K. M. Lang, and J. C. Davis, Nature (London) **413**, 282 (2001).

[2] M. Uehara, S. Mori, C. H. Chen, and S.-W. Cheong, Nature (London) **399**, 560 (1999).

[3] C. D. Ling, J. E. Millburn, J. F. Mitchell, D. N. Argyriou, J. Linton, and H. N. Bordallo, Phys. Rev. B **62**, 15096 (2000).

[4] P. G. Radaelli, R. M. Ibberson, D. N. Argyriou, H. Casalta, K. H. Andersen, S.-W. Cheong, and J. F. Mitchell, Phys. Rev. B **63**, 172419 (2001).

[5] M. Pissas and G. Kallias, Phys. Rev. B **68**, 134414 (2003).

[6] C. D. Ling, E. Granado, J. J. Neumeier, J. W. Lynn, and D. N. Argyriou, Phys. Rev. B **68**, 134439 (2003).

[7] A. Moreo, S. Yunoki, and E. Dagotto, Science **283**, 2034 (1999).

[8] J. Burgy, A. Moreo, and E. Dagotto, Phys. Rev. Lett. **92**, 097202 (2004).

[9] P. R. Sagdeo, S. Anwar, and N. P. Lalla, Phys. Rev. B **74**, 214118 (2006).

[10] K. H. Ahn, T. Lookman, and A. R. Bishop, Nature (London) **428**, 401 (2004).

[11] T. Kimura, K. Hatsuda, Y. Ueno, R. Kajimoto, H. Mochizuki, H. Yoshizawa, T. Nagai, Y. Matsui, A. Yamazaki, and Y. Tokura, Phys. Rev. B **65**, 020407(R) (2001).

[12] T. Nagai, T. Kimura, A. Yamazaki, T. Asaka, K. Kimoto, Y. Tokura, and Y. Matsui, Phys. Rev. B **65**, 060405(R) (2002).

[13] H. Nakao, T. Satoh, J. Satoh, Y. Murakami, M. Kubota, Y. Wakabayashi, H. Sawa, T. Kimura, and Y. Tokura, Physica B **329-333**, 809 (2003).

[14] R. Kajimoto, H. Mochizuki, H. Yoshizawa, T. Kimura, and Y. Tokura, Physica B **312-313**, 760 (2002).

[15] T. Nagai, T. Kimura, A. Yamazaki, Y. Tomioka, K. Kimoto, Y. Tokura, and Y. Matsui, Phys. Rev. B **68**, 092405 (2003).

[16] J. Tao, D. Niebieskikwiat, M. B. Salamon, and J. M. Zuo, Phys. Rev. Lett. **94**, 147206 (2005).

[17] J. C. Loudon and P. A. Midgley, Phys. Rev. B **71**, 220408(R) (2005).

[18] J. H. Yang and C. M. Wayman, Acta Metall. Mater. **40**, 2011 (1992).

[19] Y. H. Wen, Y. Wang, and L. Q. Chen, Acta Mater. **47**, 4375 (1999).